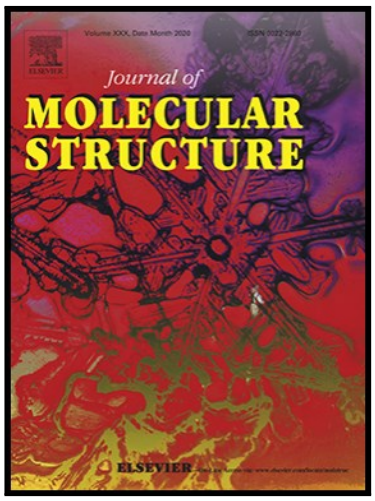


# Experimental, Spectroscopic, and theoretical investigation on structural and anticancer activities of Schiff bases derived from isonicotinohydrazide

Seema Gupta , Shivendra Kumar Pandey , Sandeep Kumar , Ram Nayan Gautam , A.K. Patel , M.K. Bharty , D. Kushwaha , A. Acharya , R.J. Butcher

PII: S0022-2860(23)01303-0
DOI: https://doi.org/10.1016/j.molstruc.2023.136212
Reference: MOLSTR 136212

To appear in: *Journal of Molecular Structure*

Received date: 31 May 2023
Revised date: 11 July 2023
Accepted date: 13 July 2023

Please cite this article as: Seema Gupta , Shivendra Kumar Pandey , Sandeep Kumar , Ram Nayan Gautam , A.K. Patel , M.K. Bharty , D. Kushwaha , A. Acharya , R.J. Butcher , Experimental, Spectroscopic, and theoretical investigation on structural and anticancer activities of Schiff bases derived from isonicotinohydrazide, *Journal of Molecular Structure* (2023), doi: https://doi.org/10.1016/j.molstruc.2023.136212

**Highlights**

- Nine Isoniazid hydrazones have been synthesized and fully characterized.
- Crystal structure and Hirshfeld surface analysis of three derivatives namely INH4, INH8, and INH9.
- DFT and TD-DFT were performed for analysis of geometry, vibrational and absorption spectra.
- Molecular docking studies reveal a strong binding affinity with MDM2 (4HG7) protein.
- In-vitro anticancer activity through MTT, AO/EtBr staining, ROS estimation, and mitochondrial membrane potential to investigate the mode of action.

# Experimental, Spectroscopic, and theoretical investigation on structural and anticancer activities of Schiff bases derived from isonicotinohydrazide

Seema Gupta[a], Shivendra Kumar Pandey[a], Sandeep Kumar[b], Ram Nayan Gautam[b], A. K. Patel[b], M. K. Bharty[a,*], D. Kushwaha[c], A. Acharya[b], R. J. Butcher[d]

[a]Department of Chemistry, Banaras Hindu University, Varanasi-221005, India.

[b]Department of Zoology, Banaras Hindu University, Varanasi-221005, India.

[c]Department of Chemistry, MMV, Banaras Hindu University, Varanasi-221005, India.

[d]Department of Chemistry, Howard University, 525 College Street NW, Washington, DC 20059, USA.

[*]**Corresponding author** E-Mail: manoj_vns2005@yahoo.co.in; mkbharty@bhu.ac.in.

**Abstract**

Isoniazid hydrazones are promising possibilities as medicines since they have preserved efficacy and are less toxic and resistant to resistance than parent Isoniazid (INH). Here, we have synthesized a series of Schiff bases (INH**1**-**9**) derived from a clinically approved antitubercular drug Isoniazid (INH). These synthesized ligands have been characterized by various spectroscopic techniques like IR, UV-vis., NMR, HRMS, etc. Moreover, single crystal of three derivatives viz. INH**4**, INH**8**, and INH**9** has been determined and they crystallize in monoclinic crystal system. Hirshfeld surface analysis has been performed to ascertain intermolecular interactions present in these compounds. The molecular geometry optimization and vibrational analysis of these compounds were performed using density functional theory (DFT) studies utilizing B3LYP/6-31++G(d, p) basis set. The TD-DFT analysis was also performed to understand electronic transitions and the nature of FMO in these compounds. There was a good correlation found between theoretical and experimental values, thereby confirming the molecular structures of synthesized compounds. Molecular docking studies were performed to obtain more insights on potential anticancer activities of these compounds along with standard anticancer drugs 5-fluorouracil and Tamoxifen against MDM2 (4HG7) protein. The outcome revealed a significant binding affinity of these compounds with target protein even better than 5-fluorouracil and comparable to Tamoxifen.

The compounds (INH**4** and INH**9**) having the strongest binding affinity with the target protein are further experimentally evaluated for their in-vitro cytotoxic action on Dalton's lymphoma cells employing MTT assay, fluorescence microscopy, and flow cytometry. $IC_{50}$ value (150 µg/ml) of this compound is equated with before-reported complexes/molecules/extracts and found it has better or comparable cytotoxicity.

***Keywords**:* Isoniazid hydrazones, Crystal Structures, DFT study, Molecular Docking Analysis, Anticancer activity, Hirshfeld Surface Analysis

## 1. Introduction

In Cancer, transformed cells divide uncontrollably and the balance between the cell cycle and cell division is lost. There are various factors that cause cancer such as genetics, heredity, chemical agents or carcinogen, UV radiation, lifestyle, etc. According to WHO, the incident rate of cancer is about 19.3 million, and 9.6 million mortality rates of cancer took place in 2021 [1]. Various treatments of cancer are present but chemotherapy is widely accepted because of their increased survival rate among all of them. Several metal complexes like cisplatin, oxaliplatin, etc are being used for the treatment of different kinds of cancer cells but they have numerous limitations. Due to acute side effects on the host body and low therapeutics porthole, the non-platinum-based metal ion is being used last few years and it gives promising results like ruthenium, gold, copper, cobalt, etc [2, 3]. In the recent era, drugs based on organic moieties are becoming an emerging trend in the treatment of cancer owing to their better bioavailability, efficacy, and fewer side effects [4].

In this era, in silico Structure-Based Drug Design (SBDD) has developed into one of the well-known, successful, and incredibly eye-catching approaches utilized by the scientific community across many disciplines for drug designing and development procedures [5]. Understanding the three-dimensional structures of the biological target protein and the ligand as well as the spatial and energetic factors that influence the binding affinities of protein-

ligand complexes are key components of this drug design strategy [6]. Isoniazid is a well-known clinically approved antitubercular drug that has isonicotinic acid hydrazide (INH) as an active component [7]. INH and its derivatives have shown its potential activity as antimycobacterial, antiviral, and antimicrobial agents [8]. INH and its derivative are successfully utilized as an excellent ligand in the preparation of metal coordinate complexes. Metal complexes containing INH and its derivative also possess medicinal activities like anti-tuberculosis, cytotoxic, anti-bacterial, anti-fungal, DNA binding, antioxidant, scavenging, and antiviral activities [9-13]. Recently, Curotto et. al. has reported Schiff bases of INH with vanillin, 5-bromovanillin, 5-chlorosalicylaldehyde, and 5-bromosalicylaldehyde and studied them theoretically [14]. Baro et. al. has reported hydrazone of isoniazid with vanillin and *o*-vanillin and performed DFT studies [15]. Dharmarajan et. al. has reported a series of 15 Isonicotinylhydrazones and found them as excellent antimycobacterial agent [16]. Rats were used to test the pharmacokinetic characteristics of the isoniazid carvone Schiff base [17].

Several INH derivatives have been synthesized and tested for antimycobacterial and anti-inflammatory activities [18, 19], but only a few are tested for their potential anticancer activity. Two INH derivatives namely N-(4-fluorobenzylidene)isonicotinohydrazide and N-(4-nitrobenzylidene)isonicotinohydrazide are reported to have antitumor activity against lung, renal, and prostate cancer [20]. Bayan et. al has reported three new Schiff bases of isoniazid with aromatic aldehydes and evaluated them for antiproliferative activity against MCF-7 cell line [21]. A review of the literature reveals that there are no reports on INH and its derivatives' ability to combat Dalton's lymphoma cells. Also, the detailed and clear characterizations (HRMS, NMR, IR, DFT, TD-DFT) of these compounds and their spectral assignments are scant. The previous reports explore INH-derived Schiff based either experimentally or theoretically, combined studies are not reported. Furthermore, only one,

two, or three derivatives are taken for studies, while we exploring nine derivatives with experimental, spectroscopic, and theoretical studies.

Herein, in view of the above, INH-derived Schiff bases were synthesized and fully characterized with the aid of different spectroscopic techniques (Uv-Vis, IR, NMR, HRMS) also by single crystal X-ray data. The physicochemical properties of these compounds (INH**1-9**) were also calculated using DFT/TD-DFT methods. The potential antiproliferative activity of INH**1-9** is investigated theoretically as well as experimentally. Molecular docking analysis of anti-cancer activities of INH**1-9** were performed with MDM2 (4HG7) protein and displayed strong binding affinities. The lead compounds (INH**4** and INH**9**) among these are further investigated for *in-vitro* anticancer activity against Dalton's Lymphoma DL cells.

## 2. Experimental

The supporting documentation includes information on chemicals, physical measurements, and X-ray crystallography.

### *2.1. Synthesis of Compounds*

In the ethanolic solution of isonicotinohydrazide (20 mmol, 2.74 g), an equimolar number of corresponding carbonyls (20 mmol) in ethanol (20 mL) was added drop-wise with constant stirring. The completion of the reaction was monitored by thin layer chromatography (TLC) ($CHCl_3$:$CH_3OH$, 8:2). After completion of the reaction, the reaction mixture was poured into crushed ice and filtered through suction. The precipitates obtained were washed twice with ice-cold distilled water and air-dried. The product obtained on recrystallization from ethanol gave the almost pure corresponding Schiff bases (INH**1-9**) (Scheme 1).

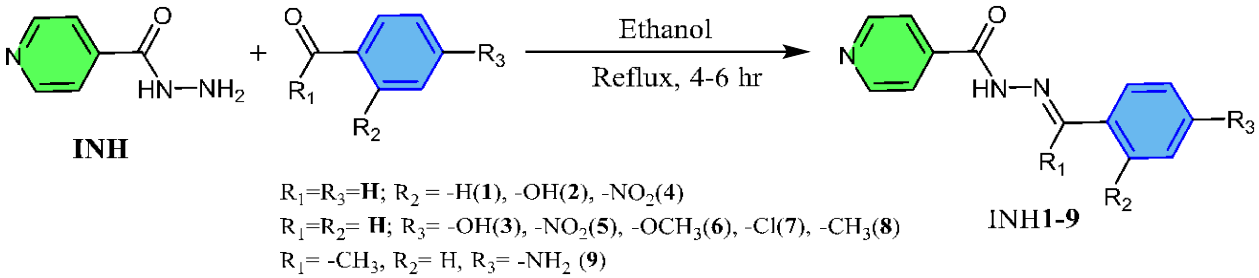


**Scheme 1**: Preparation of Schiff bases based on Isoniazid

**INH1:** Yield 82 %, m.p. 200-202; IR ($\nu$ cm$^{-1}$, KBr): 3198 $\nu$(NH); 3026 $\nu$(C-H$_{py}$); 2919 $\nu$(C-H$_{arom}$); 1693 $\nu$(C=O); 1683 $\nu$(C=N); 1598 $\nu$(C=C); 1556 $\nu$(N–H$_{bend}$); 1150 $\nu$(N–N). $^1$H NMR (600 MHz, DMSO-$d_6$) δ 12.08 (s, 1H, NH), 8.79 (d, $J$ = 4.5 Hz, 2H$_{Pyridine}$), 8.48 (s, 1H), 7.83 (d, $J$ = 4.5 Hz, 2H$_{Pyridine}$), 7.75 (d, $J$ = 7.6 Hz, 2H$_{phenyl}$), 7.47 (d, $J$ = 6.9 Hz, 3H$_{phenyl}$). $^{13}$C NMR (151 MHz, DMSO-$d_6$) δ 162.11 (C=O), 150.81, 149.52, 140.94, 134.50, 130.88, 129.32, 127.75, 122.01. UV-vis ($\lambda_{max}$, DMSO, nm) 305. HRMS (ESI, m/z): calc 226.097, found 226.095 [M+1]$^+$; calc 248.079, found 248.078 [M+Na]$^+$.

**INH2:** Yield 84%, m.p. 247-249; IR ($\nu$ cm$^{-1}$, KBr): 3348 $\nu$(OH); 3182 $\nu$(NH); 3002 $\nu$(C-H$_{py}$); 2835 $\nu$(C-H$_{arom}$); 1682 $\nu$(C=O); 1613 $\nu$(C=N); 1567 $\nu$(C=C); 1557 $\nu$(N–H$_{bend}$); 1158 $\nu$(N–N). $^1$H NMR (DMSO-$d_6$ 500 MHz) δ (ppm): δ 12.29 (s, 1H, -OH), 11.07 (s, 1H, -NH), 8.81 (d, $J$ = 4.5 Hz, 2H$_{Pyrdine}$), 8.69 (s, 1H), 7.85 (d, $J$ = 4.4 Hz, 2H, H$_{Pyrdine}$), 7.61 (d, $J$ = 7.7 Hz, 1H$_{Arom}$), 7.33 (t, $J$ = 7.8 Hz, 1H$_{Arom}$), 6.97–6.91 (m, 2H$_{Arom}$). $^{13}$C NMR (DMSO-$d_6$ 500 MHz) δ (ppm): 161.47 (C=O), 157.60, 150.53, 149.06, 140.12, 131.88, 129.33, 121.64, 119.57, 118.84. UV-vis ($\lambda_{max}$, DMSO, nm) 337. HRMS (ESI, m/z): calc 242.092, found 242.090 [M+1]$^+$ ; calc 264.074, found 264.072 [M+Na]$^+$.

**INH3:** Yield 76%, m.p. 299-301; IR ($\nu$ cm$^{-1}$, KBr): 3330 $\nu$(OH); 3233 $\nu$(NH); 3070 $\nu$(C-H$_{py}$); 2901 $\nu$(C-H$_{arom}$); 1659 $\nu$(C=O); 1599 $\nu$(C=N); 1556 $\nu$(C=C); 1518 $\nu$(N–H$_{bend}$); 1163 $\nu$(N–N). $^1$H NMR (600 MHz, DMSO-$d_6$) δ 12.29 (s, 1H, NH), 11.07 (s, 1H, OH), 8.81 (d, $J$ = 4.5 Hz, 2H), 8.69 (s, 1H), 7.85 (d, $J$ = 4.4 Hz, 2H), 7.61 (d, $J$ = 7.7 Hz, 1H), 7.33 (t, $J$ = 7.8 Hz, 1H), 6.97–6.91 (m, 2H). $^{13}$C NMR (DMSO-$d_6$ 500 MHz) δ (ppm): 161.17 (C=O), 159.59, 150.16, 148.23, 140.57, 128.98, 124.87, 121.37, 115.65. UV-vis ($\lambda_{max}$, DMSO) 318. HRMS (ESI, m/z): calc 242.092, found 242.090 [M+1]$^+$ ; calc 264.074, found 264.073 [M+Na]$^+$.

**INH4:** Yield 88%, m.p. 234-236; IR ($\nu$ cm$^{-1}$, KBr): 3193 $\nu$(NH); 3014 $\nu$(C-H$_{py}$); 2919 $\nu$(C-H$_{arom}$); 1680 $\nu$(C=O); 1562 $\nu$(C=N); 1557 $\nu$(C=C); 1519 $\nu$(N–H$_{bend}$) 1150 $\nu$(N–N). $^1$H NMR (600 MHz, DMSO-$d_6$) δ 12.35 (s, 1H), 8.82 – 8.79 (m, 2H), 8.56 (s, 1H), 8.31 (d, $J$ = 8.4 Hz,

2H), 8.02 (d, $J$ = 8.4 Hz, 2H), 7.84 (d, $J$ = 5.0 Hz, 2H). $^{13}$C NMR (151 MHz, DMSO-$d_6$) δ 162.12, 150.54, 148.20, 146.64, 140.42, 140.27, 128.36, 124.24, 121.71. UV-vis ($\lambda_{max}$, DMSO, nm) 280. HRMS (ESI, m/z): calc 271.075, found 271.079 $[M+1]^+$; calc 293.064, found 293.062 $[M+Na]^+$.

**INH5:** Yield 86%, m.p. 280-282; IR ($v$ cm$^{-1}$, KBr): 3187 $v$(NH); 3099 ν(C-$H_{py}$); 3002 ν(C-$H_{arom}$); 1683 ν(C=O); 1606 ν(C=N); 1563 ν(C=C); 1557 ν(N–$H_{bend}$); 1144 ν(N–N). $^1$H NMR (600 MHz, DMSO) δ 12.35 (s, 1H, NH), 8.82–8.79 (m, 2H), 8.56 (s, 1H), 8.31 (d, $J$ = 8.4 Hz, 2H), 8.02 (d, $J$ = 8.4 Hz, 2H), 7.84 (d, $J$ = 5.0 Hz, 2H). $^{13}$C NMR (DMSO-$d_6$ 500 MHz) δ (ppm): 162.12 (C=O), 150.54, 148.20, 146.64, 140.43, 140.27, 128.36, 124.24, 121.71. UV-vis ($\lambda_{max}$, DMSO, nm) 345. HRMS (ESI, m/z): calc 271.082, found 271.080 $[M+1]^+$.

**INH6:** Yield 78%, m.p. 166-168; IR ($v$ cm$^{-1}$, KBr): 3204 $v$(NH); 3048 ν(C-$H_{py}$); 3110 ν(C-$H_{arom}$); 2874 ν(C-$H_{methyl}$); 1657 ν(C=O); 1608 ν(C=N); 1598 ν(C=$C_{Arom}$); 1551 ν(N–$H_{bend}$); 1170 ν(N–N). $^1$H NMR (600 MHz, DMSO-$d_6$) δ 11.95 (s, 1H, NH), 8.78 (d, $J$ = 4.5 Hz, 2H), 8.41 (s, 1H), 7.82 (d, $J$ = 4.4 Hz, 2H), 7.70 (d, $J$ = 8.7 Hz, 2H), 7.03 (dd, $J$ = 8.6, 1.7 Hz, 2H), 3.80 (s, 3H, $OCH_3$). $^{13}$C NMR (151 MHz, DMSO- $d_6$) δ 161.47, 161.12, 150.33, 148.98, 140.65, 128.96, 126.60, 121.54, 114.42, 55.35. UV-vis ($\lambda_{max}$ nm, DMSO) 320. HRMS (ESI, m/z): calc 256.108, found 256.105 $[M+1]^+$; calc 278.090, found 278.088 $[M+Na]^+$.

**INH7:** Yield 80%, m.p. 216-218; IR ($v$ cm$^{-1}$, KBr): 3310 $v$(NH); 3171 $v$($CH_{py}$); 3070 ν(C-$H_{arom}$); 1667 ν(C=O); 1612 ν(C=N); 1598 ν(C=$C_{Arom}$); 1553 ν(N–$H_{bend}$); 1158 ν(N–N). $^1$H NMR (600 MHz, DMSO-$d_6$) δ 12.11 (s, 1H, NH), 8.76 (d, $J$ = 6.4 Hz, 2H), 8.43 (s, 1H), 7.79 (d, $J$ = 6.5 Hz, 2H), 7.75 (d, $J$ = 7.3 Hz, 2H), 7.52 (d, $J$ = 7.4 Hz, 2H). $^{13}$C NMR (151 MHz, DMSO-$d_6$) δ 161.67, 150.35, 147.67, 140.37, 134.84, 132.98, 129.01, 128.91, 121.52. UV-vis ($\lambda_{max}$, DMSO, nm) 310. HRMS (ESI, m/z): calc 242.090, found 242.090 $[M+1]^+$; calc 264.073, found 264.073 $[M+Na]^+$.

**INH8:** Yield 78%, m.p. 194-196; IR ($v$ cm$^{-1}$, KBr): 3253 $v$(NH); 3060 $v$($CH_{py}$); 2920 $v$($CH_{arom}$); 2840 ν(C-$H_{methyl}$); 1682 ν(C=O); 1662 ν(C=N); 1605 ν(C=$C_{Arom}$); 1568 ν(N–$H_{bend}$); 1150 ν(N–N). $^1$H NMR (600 MHz, DMSO) δ 12.00 (s, 1H, NH), 8.78 (d, $J$ = 6.2 Hz, 2H), 8.43 (s, 1H), 7.82 (d, $J$ = 6.2 Hz, 2H), 7.65 (d, $J$ = 8.2 Hz, 2H), 7.28 (d, $J$ = 8.2 Hz, 2H), 2.35 (s, 3H, $CH_3$); $^{13}$C NMR (151 MHz, DMSO) δ 161.52 (C=O), 150.33, 149.08, 140.55, 140.29, 131.33, 129.51, 127.26, 121.52, 21.01 ($CH_3$); UV-vis ($\lambda_{max}$, DMSO, nm) 309. HRMS (ESI, m/z): calc 240.113, found 240.111 $[M+1]^+$; calc 262.095, found 262.094 $[M+Na]^+$.

**INH9:** Yield 74%, m.p. 210-212; IR ($\nu$ $cm^{-1}$, KBr): 3428 $\nu(NH_2)$; 3310 $\nu(NH_2)$; 3189 $\nu$(NH); 3147 $\nu(C\text{-}H_{py})$; 2939 $\nu(C\text{-}H_{arom})$; 2854 $\nu(C\text{-}H_{Methyl})$; 1660 $\nu$(C=O); 1610 $\nu$(C=N); 1584 $\nu(C{=}C_{Arom})$; 1553 $\nu(N\text{–}H_{bend})$; 1146 $\nu$(N–N). $^1$H NMR (600 MHz, DMSO) δ 10.82 (s, 1H, NH), 8.75 (s, 1H), 8.70 (s, 1H), 7.79 (s, 1H), 7.72 (s, 1H), 7.60 (d, $J$ = 8.4 Hz, 2H), 6.58 (d, $J$ = 8.4 Hz, 2H), 5.55 (s, 2H, $NH_2$), 2.25 (s, 3H, $CH_3$). $^{13}$C NMR (151 MHz, DMSO) δ 164.18, 162.00, 159.13, 150.38, 141.67, 128.22, 122.01, 121.28, 113.41, 14.66. UV-vis ($\lambda_{max}$, DMSO, nm) 345. HRMS (ESI, m/z): calc 255.124, found 255.123 $[M+1]^+$; calc 277.106, found 277.105 $[M+Na]^+$**.**

### *2.2. Hirshfeld Surfaces analysis*

The complexes' cif files were used as input in Crystal Explorer 17.5's default Tonto mode to create the Hirshfeld Surfaces [22].

### *2.3. Quantum Chemical Calculation*

Density Functional Theory (DFT) calculations were performed using the Gaussian 09 program package [23]. The geometry optimization and frequency calculation has been accomplished through the B3LYP functional [24, 25]. The 6-311++G(d,p) basis set was employed for all calculations.

### *2.4. Molecular docking Analysis*

Using the AutoDock Tools (ADT), a molecular docking investigation of the molecule was carried out [26]. The 3D crystallographic structure of target protein MDM-2 (PDB: 4HG7) was retrieved from the Protein data bank (www.pdb.org/pdb/). All the heteroatoms were removed from the target proteins before the docking study. Next, protein is saved into PDBQT format after the addition of polar hydrogen atoms and kollman charges to it. The 2D diagram of the ligand was drawn using ACD/ChemSketch followed by 3D structure conversion and energy minimization. Gasteiger charges were added on the ligand and numbers of active torsions were set to maximum and the ligand was saved in PDBQT format. AutoGrid was used to create a grid map using grid box. For MDM-2 (4HG7), a grid box of size 40 Å X 40 Å X 40 Å, centered on X, Y, Z = - -19.723, 14.012, -8.282 was built. A grid

spacing of 0.375Å was kept for all docking runs. The Lamarckian genetic algorithm (LGA) with default parameters was implemented for carrying out molecular docking and the receptor was kept rigid. The population size was set to 150 and a maximum of 2.5 million energy evaluations were carried out. During each docking run, 10 different poses of the ligand were generated and scored using AutoDock 4.2 scoring functions and were ranked according to their binding energy. The docking result was analyzed and visualized by the discovery studio visualizer.

### *2.5. Anticancer Studies*

#### *2.5.1 MTT assay*

The cytotoxicity and cell proliferation of chemically synthesized compound INH**4** and INH**9** was assayed against Dalton's Lymphoma (DL) cells by MTT (3-(4,5-dimethylthiazol-2-yl)-2,5-diphenyltetrazolium bromide) assay as described earlier [27]. In brief DL cells ($2\times10^4$/well) were plated in 96 wells culture plate and treated with various concentration (25, 50, 100, 125, 150, 175, and 200 µg/mL) of compounds INH**4** and INH**9** for 24 hrs treatment in a 5% humidified $CO_2$ incubator at 37 temperature fter 24 h incubation, the media was removed from each well, and subsequently added 10 µL (5 mg/mL stock concentration) of MTT solution and further incubated for 4 hrs at 37 in $O_2$ incubator [28]. Aspirate the MTT solution and added 100 µL DMSO (dimethyl sulphoxide) to each well. The absorbance were then recorded at 595 nm using ELISA 680 microplate reader (Bio-Rad, USA). A concentration that led to 50% killing ($IC_{50}$) and then $IC_{50}$ values were calculated through the formula given below:

$$\%inhibition = \frac{\text{Mean OD of untreated} - \text{Mean OD of treated cells}}{\text{Mean OD of untreated cells}} x100$$

#### *2.5.2 Acridine Orange/ Ethidium Bromide (AO/EtBr) staining*

The alterations in the cellular and nuclear morphology of cancerous cells were visualized by using AO/EtBr, a double fluorescent staining vital dye [29]. In brief, DL ($1\times10^6$) cells were

treated with 75, 150, and 300 µg/mL concentrations of synthesized compound INH**9** in 6 well culture plates for 24 h under humidified environment consisting of 5% $CO_2$ at 37 ℃ temperature. After 24 hrs, the cells were washed with chilled PBS (pH 7.4), finally, 20 µL mixture of AO/EtBr dye was added to the cells and incubated for 15 min at 37 ℃. The cells were then observed under a fluorescence microscope (EVOS FL Microscopy by Life technologies).

***2.5.3 DAPI staining***

Change in the morphology of nuclear DNA was seen through DAPI staining under fluorescence microscopy. Briefly, the cells (1105) were planted on 6-well culture plates and exposed to different doses of INH9 for 24 hours (75, 150, and 300 g/mL). After treatment cells were rinsed twice with chilled PBS at 1200 rpm for 5 min. The cells were then re-suspended into PBS and finally stained with DAPI (1 µg/mL in PBS) and incubate for 15 min at 37 ℃ in the dark [29]. The image was captured and observed under fluorescence microscopy (EVOS FL Microscopy by Life Tech imaging system) for changes in the morphology of apoptotic cells.

***2.5.4 Reactive oxygen Species (ROS) estimation***

The estimation of intracellular ROS levels was assessed by using DCFH-DA staining, a fluorescent dye that determines the peroxyl, hydroxyl, and other reactive oxygen species (ROS) activity inside the cells [29]. In brief DL cells were treated with increasing concentrations (75,150 and 300 µg/mL) of compound INH**9** in 6 well culture plates for 24 h treatment. After treatment, these cells were rinsed with chilled PBS twice and stained with DCF-DA dye with a concentration of 5 µM for 30 min incubation in dark conditions. Then, the intensity of DCF (green) fluorescence cells was examined under fluorescence microscopy (EVOS FL Microscopy by Life technologies).

***2.5.5 Mitochondrial Membrane Potential (MMP)***

Mitochondria play a significant role in the process of apoptosis, during this process loss in mitochondrial membrane potential (ΔΨm) is well reported [29]. In this present study, the effect of compound INH**9** on mitochondrial membrane potential of DL cells was assessed by Flow cytometry using rhodamine-123 fluorescent dye. Briefly, DL cells ($6\times10^5$) were treated in 6 well culture plate for 24 hrs treatment in a humidified chamber having 5% $CO_2$ at 37 with different concentrations (75, 150, and 300 µg/mL) of compound INH4. After 24 hrs, the treated cells were washed with chilled PBS and fixed cells in 4% paraformaldehyde for 20 min, then cells were stained with rhodamine-123 at a final concentration of 10 µM and incubated for 30 min in dar condition at 37 . The stained images were photographed under fluorescence microscopy (EVOS FL Microscopy by Life Technologies) and analysed by Image (J) Software [29].

## 3. Results and Discussion

The compounds INH**1-8** were prepared by refluxing a mixture of Isoniazid and corresponding carbonyls in ethanol. The synthesized compound INH**1-9** has been characterized by various spectroscopic techniques including IR, NMR, and HRMS. The HRMS spectrum of compounds has been given in supporting Fig. 28-36. The compounds INH**1-9** have been found to be air-stable that can be kept at room temperature for a longer time without any sign of decomposition. Compounds INH**1-9** were found to be soluble in polar organic solvents (ethanol, methanol, DMSO). To understand the potential anti-cancer activity of INH**1-9**, the molecular docking study of the compound was executed with p53-associated MDM2 (4HG7) protein. The antiproliferative activity of compounds INH**9** have been examined on Dalton's lymphoma cells and determined by standard MTT assay.

### 3.1 Electronic Absorption Spectra

The electronic absorption spectra of INH**1-9** were recorded in $10^{-4}$ M DMSO solution. Compound INH**1-9** displays bands at 305, 337, 318, 280, 342, 320, 310, 309, and 345 nm, respectively (Fig. 1a). In order to test the nature of transitions, UV-vis. Spectra of INH**9** have

been recorded in less polar ethanol than DMSO and show the band at 326 nm (Fig. 1b). The bathochromic shift observed upon changing solvent polarity suggests that observed transitions may be assigned to π →π* transition [30].

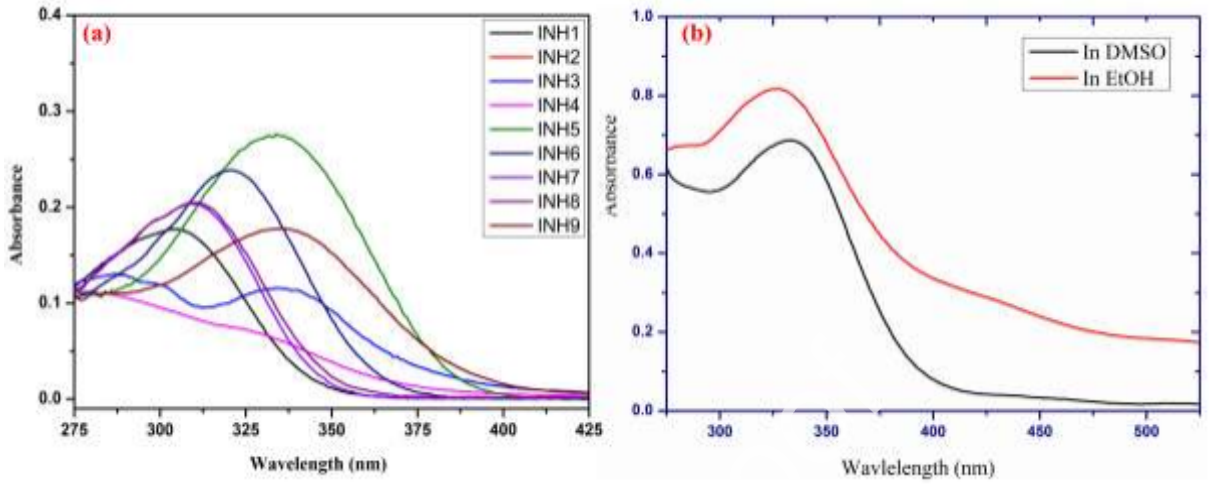


**Fig. 1**: Electronic absorption spectra of (a) INH**1-9** in $10^{-4}$ M DMSO. (b) INH**9** in $10^{-5}$ M DMSO and ethanol.

### 3.2 IR Spectrum

The IR spectrum of INH**1-9** showed the characteristic bands of NH, CH, C=O, C=N, C=C, and N-N stretching vibrations. The stretching modes of N-H (amide) were observed in the range 3187-3310 $cm^{-1}$. The carbonyl stretching frequency was found in the range 1657-1693 $cm^{-1}$, indicating the presence of an amide group. The $CH_{aromatic}$ stretching vibrations were observed in range of 2919-3171 $cm^{-1}$. In addition, INH**6**, INH**8** and INH**9** also shows $CH_{methyl}$ vibrations bands at 2874, 2840, and 2854 $cm^{-1}$, respectively Further, ν(N-N) stretching vibrations were observed at 1150, 1158, 1163, 1150, 1144, 1170, 1158, 1150, and 1146 $cm^{-1}$, respectively. The ν( = ) and ν( =N) stretching vibrations were observed in their characteristic range (Supporting Fig. 1-9) [14, 15].

### 3.3 $^{1}$H and $^{13}$C NMR spectrum

The $^{1}$H and $^{13}$C NMR spectra of INH**1-9** were recorded in DMSO-$d_6$. $^{1}$H NMR spectrum of INH**1-9** shows highly deshielded signals at δ 12.08, 12.29, 11.88, 12.40, 12.35, 11.95, 12.13,

12.00, 10.82, respectively, ppm due to NH proton of the amide group. The OH proton of INH2 and INH3 were observed at δ 11.07 and 10.00 ppm, respectively. The aromatic ring protons were observed in range of δ 6.57-8.90 ppm. The aromatic protons were most shielded in INH**9** and deshielded in INH**4** owing to the presence of -$NH_2$ and -$NO_2$ groups in them. The amine group ($NH_2$) protons in INH**9** were found at δ 5.55 ppm. The -$CH_3$ protons in INH**6**, INH**8** and INH**9** were observed at δ 3.80 ($OCH_3$), 2.35, and 2.25 ppm, respectively (Fig. 3). $^{13}C$ NMR spectrum of INH**1-9** shows a signal at δ 161.75 and 158.84 ppm due to C=O, respectively suggesting the presence of carbonyl carbon. Aromatic carbons were observed in the range aromatic range of δ 113.59-150.38 ppm. The methyl (-$CH_3$) carbon present in INH6, INH8, and INH9 were observed at δ 55.35 (-$OCH_3$), 21.01, and 14.84 ppm (Supporting Fig. 10-27).

**3.4 Crystal Structure description**

The structure and geometry of the synthesized compounds INH**4**, INH**8**, and INH**9** were analysed by X-ray diffraction technique which confirms exactly the molecular structure of the compounds. Table 1 lists the specific crystallographic parameters and structural refinement information for the compounds INH**4**, INH**8**, and INH**9**. Some selected bond lengths and bond angles for compounds INH**4**, INH**8**, and INH**9** has been given in Table 2. Hydrogen bonding parameters for compounds INH**4**, INH**8**, and INH**9** are listed in Supporting table 1, 2 and 3 respectively.

**Table 1**: Structural refinement and crystal parameters for compounds INH**4**, INH**8**, and INH**9**

| Parameters | **INH9** | **INH8** | **INH4** |
|---|---|---|---|
| Empirical formula | $C_{14}H_{14}N_4O$ | $C_{14}H_{15}N_3O_2$ | $C_{13}H_{10}N_4O_3$ |
| Formula weight | 254.29 | 257.29 | 270.25 |
| Crystal system | Monoclinic | Orthorhombic | monoclinic |
| Space group | P $2_1$/n | *P* $2_1$ $2_1$ $2_1$ | P $2_1$/c |
| T (K) | 293(2) | 293(2) | 293(2) |

| | | | |
|---|---|---|---|
| λ, Mo Kα (Å) | 1.54178 | 0.71073 | 0.71073 |
| a (Å) | 7.9156(5) | 6.3750(4) | 7.4828(2) |
| b (Å) | 5.3548(4) | 7.4205(5) | 10.8993(3) |
| c (Å) | 29.7103(16) | 28.2188(18) | 15.4678(4) |
| α (°) | 90 | 90 | 90 |
| β (°) | 95.47(5) | 90 | 94.880(2) |
| γ(°) | 90 | 90 | 90.00 |
| V, ($Å^3$) | 1253.58(14) | 1334.91(15) | 1256.94(6) |
| Z | 4 | 4 | 4 |
| $\rho_{calcd}$ ($g/cm^3$) | 1.347 | 1.280 | 1.428 |
| μ ($mm^{-1}$) | 0.722 | 0.088 | 0.106 |
| F (000) | 536 | 544 | 560 |
| Crystal size($mm^3$) | 0.14x0.12x0.10 | 0.34x0.26x0.18 | 0.18x0.12x0.05 |
| θ range for data collections (°) | 5.671 -72.214 | 2.838-27.069 | 2.640-26.731 |
| Index ranges | $-9 \leq h \leq 9$ | $-8 \leq h \leq 7$ | $-9 \leq h \leq 9$ |
| | $-6 \leq k \leq 5$ | $-9 \leq k \leq 9$ | $-13 \leq k \leq 13$ |
| | $-27 \leq l \leq 36$ | $-34 \leq l \leq 35$ | $-19 \leq l \leq 18$ |
| No. of reflections collected | 4487 | 7645 | 19298 |
| No. of independent reflections ($R_{int}$) | 2422 | 2573 | 2645 |
| No. of data/restrains/ parameters | 2422 / 0 / 173 | 2573/0/176 | 2645/0/185 |
| Goodness-of-fit on $F^2$ | 1.024 | 0.988 | 1.056 |
| $R_1$[a], $wR_2$[b] [(I>2σ(I)] | 0.0551, 0.1497 | 0.0532, 0.1057 | 0.0470, 0.1198 |
| $R_1$[a], $wR_2$[b] (all data) | 0.0667, 0.1651 | 0.0928, 0.1265 | 0.0629, 0.1365 |
| Largest difference in peak /hole ($e.Å^{-3}$) | 0.239, -0.310 | 0.184, -0.183 | 0.189, -0.225 |

**Table 2**: Selected bond length for compounds INH**4**, INH**8**, and INH**9**

| **Bond Lengths(Å)** | **INH4** | **INH8** | **INH9** |
|---|---|---|---|

| | Exp | Calc. | Exp. | Calc. | Exp. | Calc. |
|---|---|---|---|---|---|---|
| O(1)-C(1) | 1.2139(18) | 1.210 | 1.226(4) | 1.212 | 1.217(2) | 1.213 |
| N(2)-C(1) | 1.3546(19) | 1.388 | 1.338(4) | 1.382 | 1.351(2) | 1.382 |
| N(2)-N(3) | 1.3726(16) | 1.351 | 1.390(3) | 1.359 | 1.3936(19) | 1.361 |
| N(3)-C(7) | 1.268(2) | 1.281 | 1.274(4) | 1.280 | 1.288(2) | 1.290 |
| C(7)-C(8) | 1.468(2) | 1.470 | 1.459(4) | 1.461 | 1.487(2) | 1.478 |
| C(1)-C(2) | 1.502(2) | 1.505 | 1.494(5) | 1.507 | 1.502(2) | 1.508 |
| C(9)-N(4) | 1.458(2) | 1.479 | - | - | - | - |
| C(11)-C(14) | - | - | 1.516(5) | 1.508 | - | - |
| C(7)-C(14) | - | - | - | - | 1.489(3) | 1.513 |
| C(11)-N(4) | - | - | - | - | 1.380(2) | 1.389 |

**Table 3**: Selected bond angles for compounds INH**4**, INH**8**, and INH**9**

| **Bond Angle (°)** | **INH4** | | **INH8** | | **INH9** | |
|---|---|---|---|---|---|---|
| | Exp. | Calc. | Exp. | Calc. | Exp. | Calc. |
| C(1)-N(2)-N(3) | 118.38(12) | 120.842 | 118.4(3) | 121.183 | 118.10(15) | 120.34 |
| C(7)-N(3)-N(2) | 116.05(13) | 117.177 | 115.1(3) | 117.014 | 116.58(15) | 118.647 |
| N(3)-C(7)-C(8) | 118.67(14) | 119.458 | 121.1(3) | 122.303 | 114.59(16) | 116.503 |
| O(1)-C(1)-N(2) | 123.08(14) | 123.509 | 123.6(3) | 124.022 | 124.11(16) | 124.302 |
| O(1)-C(1)-C(2) | 121.11(14) | 122.472 | 120.1(3) | 122.073 | 121.27(16) | 121.820 |
| N(2)-C(1)-C(2) | 115.80(13) | 114.015 | 116.3(3) | 113.922 | 114.58(16) | 113.876 |

### 3.4.1 INH4

Fig. 2a displays the ORTEP diagram for compound INH**4** together with the crystallographic numbering system and thermal ellipsoids at the 30% probability level. The molecular structure of **2** crystallizes in the monoclinic system with the *P* 21/*n* space group. It is discovered that the dihedral angle between the pyridine ring (C2, C3, C4, N1, C5, and C6) and the phenyl ring (C2, C3, C4, N1, C5, and C6) is 73.20°, indicating that both rings are perpendicular with regard to one another. The C=O bond, which has a bond length of 1.217(2), is solely a double bond that participates in the expansion of supramolecular

structures *via* intermolecular hydrogen bonding. The mean plane of the amide group is nearly coplanar to the planes of their adjacent pyridine ring with dihedral angles of 38.92°. The C1-N2 and C7-N3 bond lengths are 1.355(2) and 1.268(2) Å, respectively which lie between the typical single carbon-nitrogen and double carbon-nitrogen bonds and are well agreed with other similar reported compounds [14]. The structure of INH**4** is stabilized by intermolecular C-H···O hydrogen bonding interactions found between CH hydrogens of the methyl group and phenyl ring and the carbonyl oxygen of another nearby unit of compound INH**4**. The structure is also stabilized by N-H···O hydrogen bonding interactions between the NH hydrogen of the hydrazine moiety of the compound and the carbonyl oxygen atoms of the compound (Supporting Fig. 37). Further, the N-H···N hydrogen bonding also stabilized the structure, which is present between the NH hydrogen of the amine group and pyridine ring nitrogen of another unit of the compound. In addition, INH**4** is stabilized by stacking interaction between pyridine ring and phenyl ring (Fig. 2b).

**3.4.2 INH8**

The ORTEP diagram together with the crystallographic numbering scheme of compound INH4 is shown in Fig. 2c with thermal ellipsoids at the 30 % probability level. The molecular structure of **1** crystallizes in the Orthorhombic system with $P\,2_1\,2_1\,2_1$ space group. One water molecule is also co-crystallized with compound INH**8** and interlinked through intermolecular hydrogen bonding. The dihedral angle between the pyridine ring (C2, C3, C4, N1, C5, and C6) and phenyl ring (C8, C9, C10, C11, C12, and C13) is found to be 16.40° indicating that both rings are nearly coplanar with respect to each other. The C=O bond having bond length 1.217(2) Å is purely a double bond that takes part in the construction of supramolecular architectures through intermolecular hydrogen bonding. The C1-N2 and C7-N3 bond lengths are 1.351(2) and 1.289(2) Å, respectively, due to the extensive delocalization of π electron over the C(1)–N(2)–N(3)–C(7) linkage. These bond distances lie between the typical ─N

and C=N values and are very similar to other reported hydrazone compounds 1.394(2), 1.299(2) Å [14, 15]. The N(2)-N(3)-C(7) bond angle is (115.10(10)$^{o}$) showing nearly planar $sp^2$ hybridized behaviour of N3. The mean plane of the amide group is nearly coplanar to the planes of their adjacent pyridine ring with dihedral angles of 32.92$^{o}$ separating their groups to avoid steric hindrance. In the solid state, the structure of compound **1** is stabilized by C-H···O and O-H···O, and intermolecular hydrogen bonding occurs between the CH hydrogen of phenyl ring /OH hydrogen of water molecules and the carbonyl oxygen of another unit of the compound moiety leading to the formation of a supramolecular architecture (Supporting Fig. 38). In addition, the structure is further stabilized by N-H···O hydrogen bonding between the NH hydrogen of hydrazine moiety of the compound and oxygen atoms of water molecules (Supporting Fig. 38).

**3.4.3 INH9**

Fig. 2d displays the molecular structure of INH**9** along with the atomic numbering scheme and thermal ellipsoids at the 30% probability level. INH**9** crystallizes in the monoclinic system with space group *P*21/*c*. The dihedral angle between the nitro phenyl ring (C8, C9, C10, C11, C12, and C13) and pyridine ring (C2, C3, C4, N1, C5, and C6) is observed to be 8.11° representing that both rings are nearly planar with respect to each other. The mean plane of the carbo amide group is approximately coplanar to the planes of their adjacent pyridine ring with dihedral angles of 15.39$^{o}$ separating their groups to escape steric hindrance. The C1-N2 and C7-N3 bond lengths are 1.355(2) and 1.268(2) Å, respectively, due to the wide delocalization of π electron over the (1)–N(2)–N(3)–C(7) moiety. These distances lie between the typical ─N single bond and =N double bond values and are well agreed with other reported compounds [31]. The N(2)-N(3)-C(7) bond angle is 116.09(13) $^{o}$ showing nearly planar $sp^2$ hybridized behaviour of N3. The C=O bond length is 1.2117(18) Å which is a nearly double bond that involves the generation of a linear chain through

intermolecular hydrogen bonding. In the solid state, the structure of compound **3** is stabilized by C-H···S intermolecular hydrogen bonding occurs between the CH hydrogen of the phenyl ring and nitrogen atoms of the nitro group of another unit of the compound leading to the formation of a 2D framework (Supporting Fig. 39).

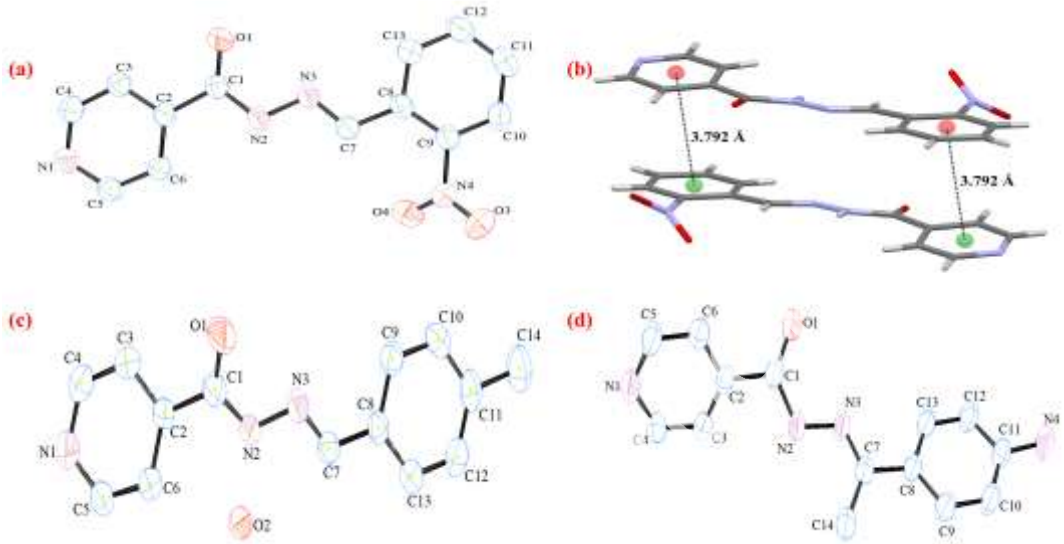


**Fig. 2:** ORTEP diagram of (a) INH4, (c) INH8 and (d) INH9 at 30 % thermal ellipsoid, (d) π···πstac ing interaction in INH4

### 3.5 Hirshfeld surfaces Analysis

Hirshfeld surfaces (HS) for INH**4**, INH**8**, and INH**9** were generated employing the default Tonto code. Fig. 4 displayed the HS over the $d_{norm}$. The $d_{norm}$ surface's red, white, and blue patches, respectively, depict areas where external atoms are in close proximity, moderate closeness, and a distance away [32]. The dnorm of compounds INH4, INH8 and INH9, shows intense red spots corresponding to strong intermolecular interactions O···H/H···O and N···H/H···N that stabilizes them (Fig. 5). The nature and kind of intermolecular interactions seen in the INH4, INH8, and INH9 were quantitatively summarized using 2-D fingerprint plots, which were resolved from the original 3-D dnorm surfaces were shown in supporting fig. 40-42. Fig. 4d shows the percentage contribution of contacts, including their reciprocal contact  The N···H/H···N contact in dominant interaction in INH8 and INH9 whereas

O···H/H···O is dominant in INH4. In addition, there is the presence of C···C (pi-pi) interaction (3.0%) in INH**4** [33].

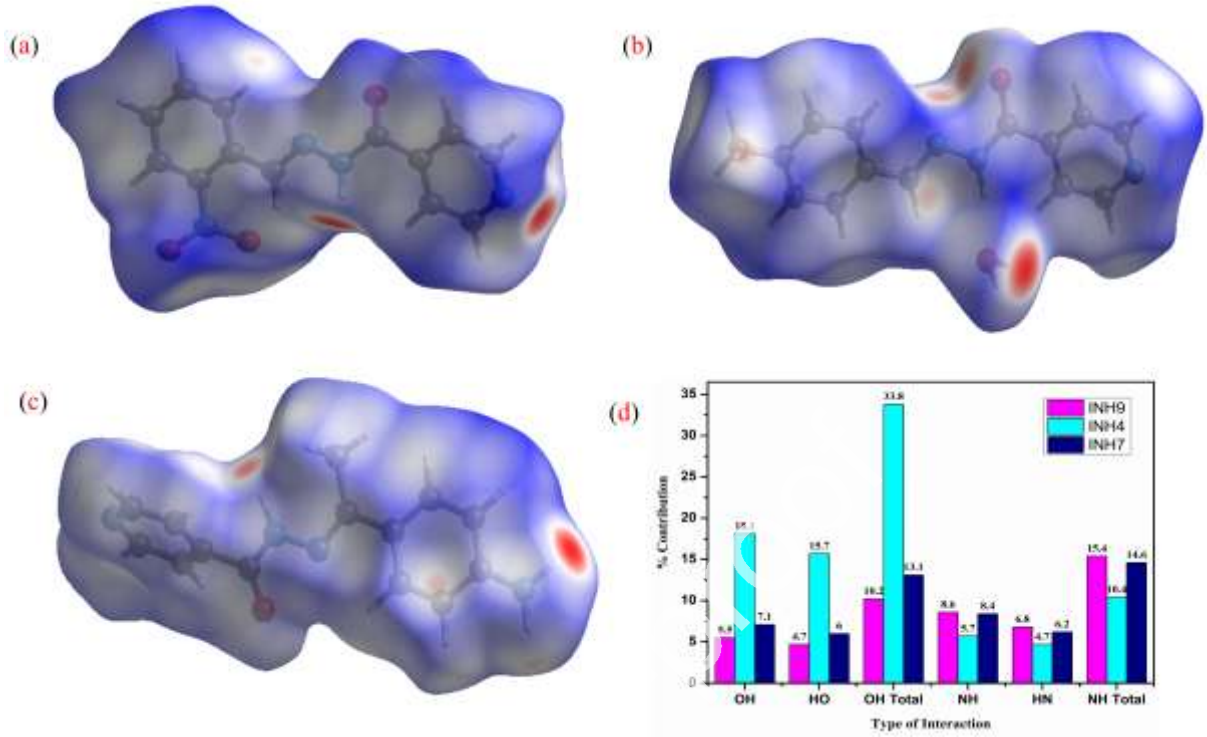


**Fig. 3**: $d_{norm}$ surfaces of (a) INH4, (b) INH8, and (c) INH9 and (d) % of individual contribution.

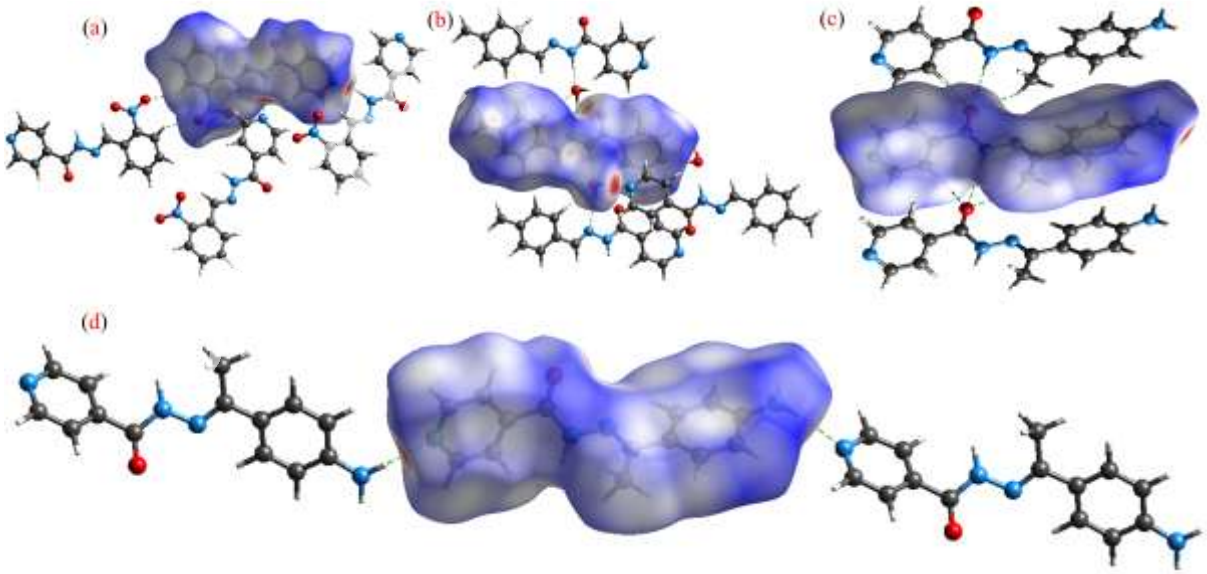


**Fig. 4**: Showing type of Intermolecular interactions present (a) C-H···O and N-H···N in INH**4**, (b) O-H···O and N-H···O in INH**8**, (c) C-H···O and N-H···O in INH**9** and (d) N-H···N in INH**9**

### 3.5. DFT Studies

The geometry optimization for INH derived Schiff bases has been carried out to get insights about bond parameters and vibrational frequencies. The geometry of INH**1-9** have been optimized in the gas phase through B3LYP/6-311++G(d,p) basic set. The optimized structure of INH**1-9** has been shown in supporting materials (Supporting Fig. 43). The selected bond lengths and bond angles of the optimized structures INH4, INH8, and INH9 has been compared with their corresponding experimental data and shown in table 2 and 3 respectively. For rest of the derivatives selected bond length and angles has been given in supporting Tables 4 and 5.

The vibrational frequencies were also calculated by DFT/B3LYP levels with 6-311-G(+,+) basis set. The theoretical vibrational spectra of INH**1-9** have been shown in supporting material (Supporting Fig. 44-52). The comparison of important experimental and calculated vibrational bands have been given in the Supporting material. The observed experimental and theoretical vibrational frequencies were assigned for different modes of vibrations, which have been presented in supporting Tables 6 and 7. The disagreement observed between the theoretical and experimental values is since the DFT calculations have been done for an isolated molecule in the gas phase, while IR spectra were recorded in the solid phase with KBr pellets. Other factors such as hydrogen bonding interactions especially in $NH_2$, C=O, group vibrations due to C=O/H-N interactions, and electron correlation effects that can distort symmetry and normal values were also responsible for disagreement observed [34].

**3.6 TD-DFT Studies**

Furthermore, time-dependent density functional theory studies are also performed to get an in-depth understanding of electronic transitions involved in INH**1-9**. The TD-DFT studies has been performed using CPCM model with DMSO as solvent. Results from TD-DFT and experimental UV-vis spectra were found to be highly correlated and band assignments are

summarized in Table 4. Among the various transition observed theoretically in molecules INH**1-9** theoretically only transitions having highest oscillator strength are chosen and shown in table 3 since these transitions having highest oscillator strength have dominant contribution in electronic transition. For compound INH9 calculated absorption bands in DMSO and ethanol are shown by the green line while corresponding experimental bands are shown by blue lines in Supporting Fig. 71. A few deviations were described to the negligence of anharmonicity in the B3LYP method [35].

**Table 4:** Comparative study of experimental UV–visible transitions with theoretical transitions obtained from td b3lyp/6-311++g(d,p) scrf=(cpcm, solvent=dmso/ethanol) calculation in INH**1-9** with their assignments

| **Compound** | $\lambda_{max}$ (Exp ) nm | $\lambda_{max}$ ( alc ) nm | **f** = Oscillator strength | **Transitions** | **Assignments** |
|---|---|---|---|---|---|
| INH1 | 305 | 328 | 0 7400 | HOMO→LUMO | π→ π * |
| INH2 | 337 | 341 | 0 5537 | HOMO→LUMO | π→ π * |
| INH3 | 318 | 348 | 0 4551 | HOMO→LUMO+1 | π→ π * |
| INH4 | 280 | 313 | 0 4371 | HOMO→LUMO+1 | π→ π * |
| INH5 | 342 | 379 | 0 8325 | HOMO→LUMO | π→ π * |
| INH6 | 320 | 355 | 0 7198 | HOMO→LUMO | π→ π * |
| INH7 | 310 | 330 | 0 6631 | HOMO→LUMO | π→ π * |
| INH8 | 309 | 338 | 0 7556 | HOMO→LUMO | π→ π * |
| INH9 (DMSO) | 345 | 389 | 0 5186 | HOMO→LUMO | π→ π * |
| INH9 (ethanol) | 326 | 306 | 0 4281 | HOMO→LUMO+1 | π→ π * |

The HOMO and LUMO (frontier molecular orbitals) are important for a molecule's chemical reactivity, optical polarizability, and chemical hardness-softness. To ascertain how the charge is transferred within the molecule, HOMO and LUMO studies are also used. The HOMO-LUMO gap of a molecule also determines the chemical hardness and softness of the molecule. The large HOMO-LUMO gap signifies a hard molecule whereas a small HOMO-LUMO gap indicates a soft molecule. The stability and reactivity of molecules also relate with HOMO-LUMO gap, molecules with small HOMO-LUMO gaps are more reactive molecules than molecules with large HOMO-LUMO gaps. Hard systems are often small and significantly less polarizable than soft systems, which tend to be big and highly polarizable [36, 37].

HOMO-LUMO analysis of lead compound INH9 (based on anticancer and docking study discussed in later sections) has been performed and shapes of HOMO, LUMO and the energy gap between them is shown in Fig 5. HOMO of compound INH9 shows that electron density is mainly localized over the aniline ring, while LUMO of INH9 shows that the electron density would be localized over the pyridine ring. Thus, the electronic transition from the ground state to the excited state of INH9 attributes to $\pi \rightarrow \pi^*$ transition The HOMO-LUMO energy gap of 2.8291 eV was found in INH**9**. This smaller energy gap between HOMO and LUMO suggests compound INH**9** is soft and highly reactive.

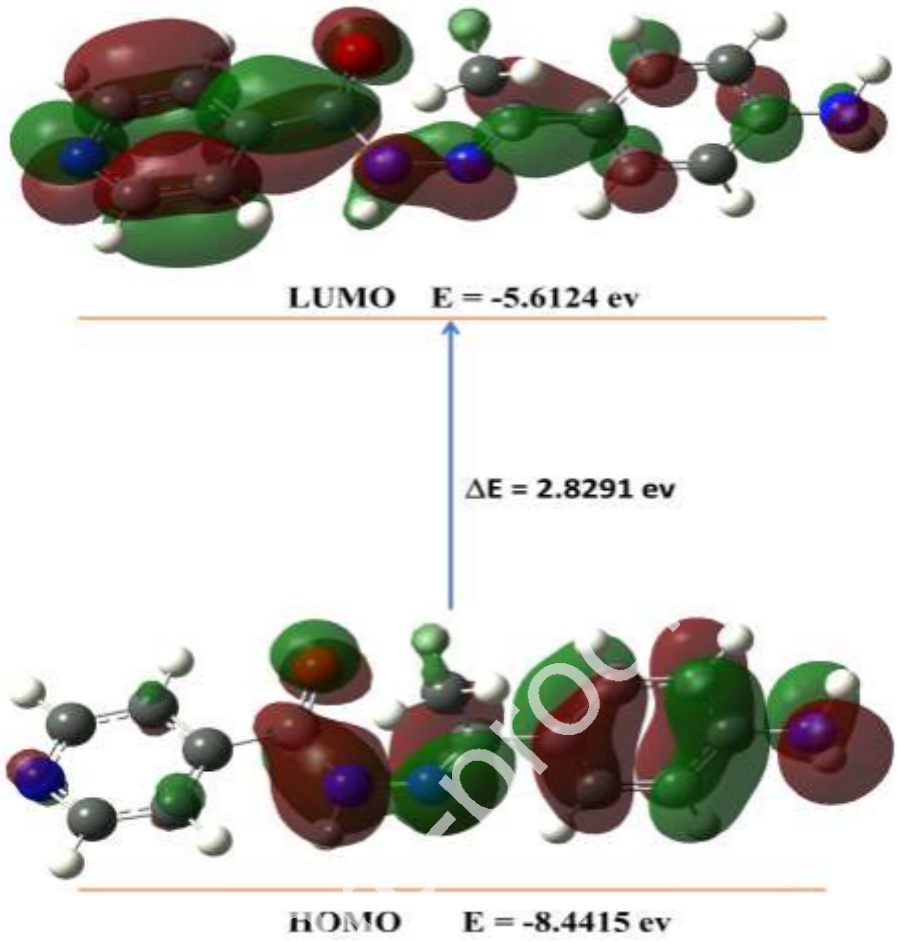


**Fig. 5**: Diagram shapes and the energy difference between HOMO and LUMO of INH9

**3.7 Molecular docking description:**

In order to understand the potential anti-cancer activity of INH and its Schiff base derivatives, molecular docking study of these synthesized compounds were performed with MDM2 (4HG7) protein [38]. The tumour suppressor protein p53, a key protein that prevents tumour formation and growth by inducing cell cycle arrest, and apoptosis. At the incident of cancers, the p53 activity is lost either by mutation or by the inactivation due to the overexpression of the main endogenous negative regulator, murine double minute 2 (MDM2). As the inhibitors of p53–MDM2 interaction restores the p53 activity, we studied the binding affinity of INH and its derivative with MDM2 (4HG7) [38, 39]. The binding affinity INH and its Schiff base derivatives (INH1-9) along with standard anticancer drugs 5-fluorouracil and tamoxifen with MDM2 obtained through molecular docking simulation has

been given in table 5. The INH1-9 are found to inhibit the function of target protein than 5-Fluorouracil and have comparable result more strongly with tamoxifen. The INH derivative INH9 has been found to strongest binding affinity among others. Thus, its detailed docking analysis is studied further. The docked diagram of other derivatives and standard drugs has been shown in *supporting material* (Supporting Fig. 72-82).

INH9 showed effective binding within the binding pocket of MDM-2 via two hydrogen bonds and six hydrophobic interactions having an overall free binding energy of -6.7 kcal/mol. The $–NH_2$ group behaved as a hydrogen donor to form H-bond with the residue Tyr100 (bond length 2.34 Å), whereas pyridyl nitrogen acted as an acceptor to H-bond with Gln59 (bond length 2.10 Å). Furthermore, INH9 stabilized itself in the binding pocket through the al yl, π-al yl, π-donor H-bond, van der Waals and amide- π stac ed interactions with the residues Lys51, Leu54, Gly58, and Gln59, respectively (Fig. 6).

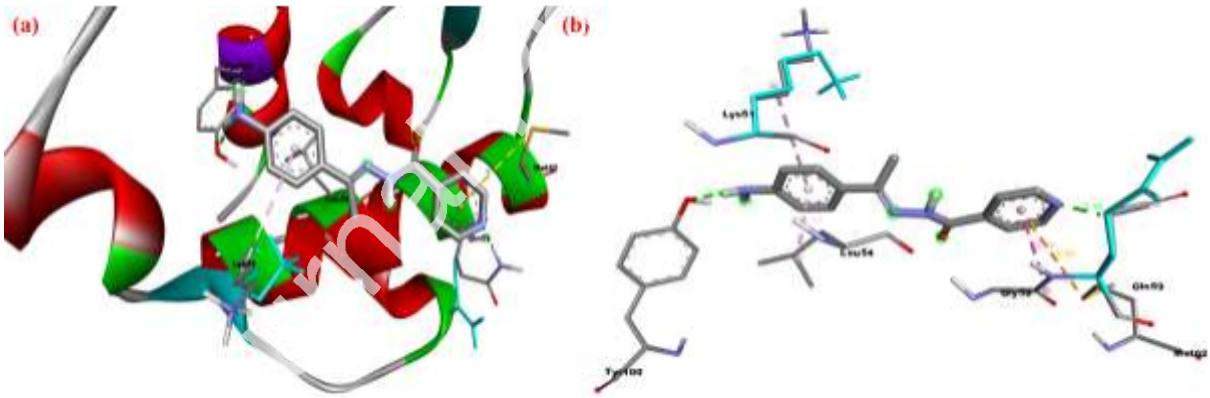


**Fig. 6**: 3D docked pose of the INH9 in the active site of target MDM-2 (pdb: 4HG7) (a) with receptor protein (b) with receptor amino acids

**Table 5**: Binding scores of Compounds INH1-9 with target protein

| S.N. | Compound | Binding Affinity (Kcal/mol) |
|---|---|---|
| 1. | INH | -5.1 |
| 2. | INH1 | -6.2 |
| 3. | INH2 | -6.1 |
| 4. | INH3 | -6.3 |

| | | |
|---|---|---|
| 5. | **INH4** | **-6.5** |
| 6. | INH5 | -6.5 |
| 7. | INH6 | -6.4 |
| 8. | INH7 | -6.3 |
| **9.** | **INH8** | **-6.7** |
| 10. | 5-FU | -4.2 |
| 11. | Tamoxifen | -7.1 |

### 3.7 Antitumor Studies

Based on docking studies, we check in vitro anticancer potential for the lead compounds INH**4** and INH**9** having the highest binding affinity with MDM2 (4HG7) protein.

#### *3.7.1 INH derivatives inhibit the proliferation of Dalton's Lymphoma cells*

The anti-proliferative activity of compound INH**4** and INH**9** were determined by standard MTT assay, they react with succinate dehydrogenase in presence of NAPDH and forms formazan crystal. After reacting with DMSO, they provide cell viability. After 24 hrs treatment, the viability of Dalton's lymphoma cells decreased in a dose-dependent manner is shown in Fig. 7. The value of $IC_{50}$ for INH9 was obtained at 150 µg/mL (Fig 7b), whereas INH**4** does not show any appreciable result (Fig. 7a). Further studies of this compound for anticancer activity at a low and higher dose of $IC_{50}$ were ta en as 75 µg/ml and 300 µg/mL, respectively. Thus, the rest of the anticancer studies have been performed for the lead compound INH**9** **[**29**]**.

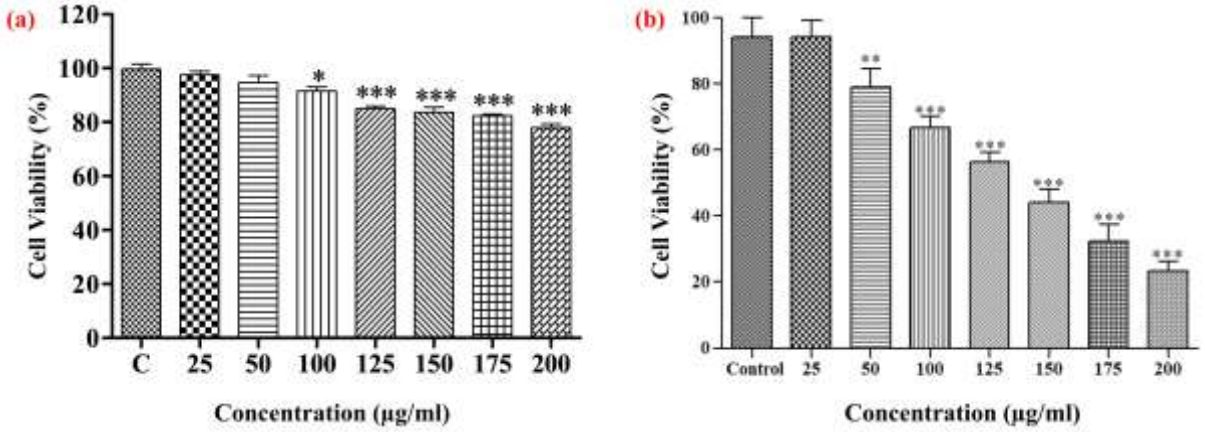


**Fig. 7:** Anti-proliferative effect of compound INH**4** and INH**9** on cell viability in DL cells at several concentration ranges from (0, 25, 50, 100, 125, 150, 175, 200 µg/ml) for 24 h treatment. Results are represented as a mean ± SD of three independent experiments indicates **$p < 0.01$, *** $p < 0.001$ as compared to control.

### 3.7.2 Acridine orange/ ethidium bromide (AO/EB) dual staining

Apoptosis is one of the most studied processes in biological science. During this process cell shrinkage, nuclear condensation, blebbing of the plasma membrane, and the organelles become more compactly packed [43]. DL cells were treated with INH**9** compound for 24 h treatment using dual AO/EtBr fluorescent staining, assessed the induction of apoptosis under fluorescence microscopy (Supporting Fig. 83). These results revealed that no significant apoptosis was found in the control (untreated) group while treated cells exhibited a number of yellowish-green with disrupted membrane integrity showing early apoptosis in lower concentrations. Late-stage apoptotic cells display orange/red fluorescence with the condensed nucleus and fragmented DNA in the higher concentration of treated cells. Necrotic cells were also observed with the increase in drug concentration and showed uneven orange-red fluorescence at their outer surface.

### 3.7.3 Assay for Nuclear Morphology

DAPI (4,6-diamidino-2-phenylindole) is a fluorescent staining dye that strongly binds to the A-T-rich repeats of DNA sequences. DAPI evaluates the condensation and fragmentation of

DNA and changes in the morphology of apoptotic cells [32] The Dalton's Lymphoma cells were treated with compound INH9 for 24 hrs treatment. In this study, DAPI staining depicts the morphological alterations associated with apoptosis. The control (untreated) cells showed normal nuclear morphology, remain intact and evenly shaped however treated cells displayed cell shrinkage, condensed chromatin, and nuclear fragmentation into discrete fragments resulted in a concentration-dependent manner (Supporting Fig. 84).

**3.7.4 ROS Estimation**

The fluorescent product DCF (2', 7' dichlorofluorescein) was obtained from the oxidation of DCFH-DA in the presence of ROS [29]. The amount of ROS produced by the dead cells was relatively proportional to the intensity of spotted DCF (green) fluorescence. ROS production at a minimal (basic) level initiates cell growth, proliferation, and differentiation but rather than above this level promotes the activation of apoptotic pathways. The effect of compound INH9 on the condition of ROS production in DL cells for 24 hrs treatment was analysed by DCF-DA staining shown in Supporting Fig. 85. The intensity of green fluorescence was detected in a concentration-dependent fashion (75,150 and 300 μg/ml) in treated cells. The compound INH9 displayed that the intracellular ROS production increased significantly as compared to the control. For statistical analysis, ImageJ (NIH, USA) and GraphPad Prism 5.0 software were used.

**3.7.5 INH9 decayed mitochondrial membrane potential (ΔΨm)**

To investigate the induction of intrinsic apoptotic pathway loss in mitochondrial membrane potential is the crucial event; changes in the mitochondrial membrane potential were assessed by using rhodamine-123 fluorescent dye detected by flow cytometry in a concentration-dependent manner [29]. The present outcome revealed that compound INH9 induced a significant decrease in the membrane potential of mitochondria, which showed that

compound INH9 prompt apoptosis in DL cells as compare to control (untreated cells) in Fig. 8. For statistical analysis, ImageJ (NIH, USA) and GraphPad Prism 5.0 software were used.

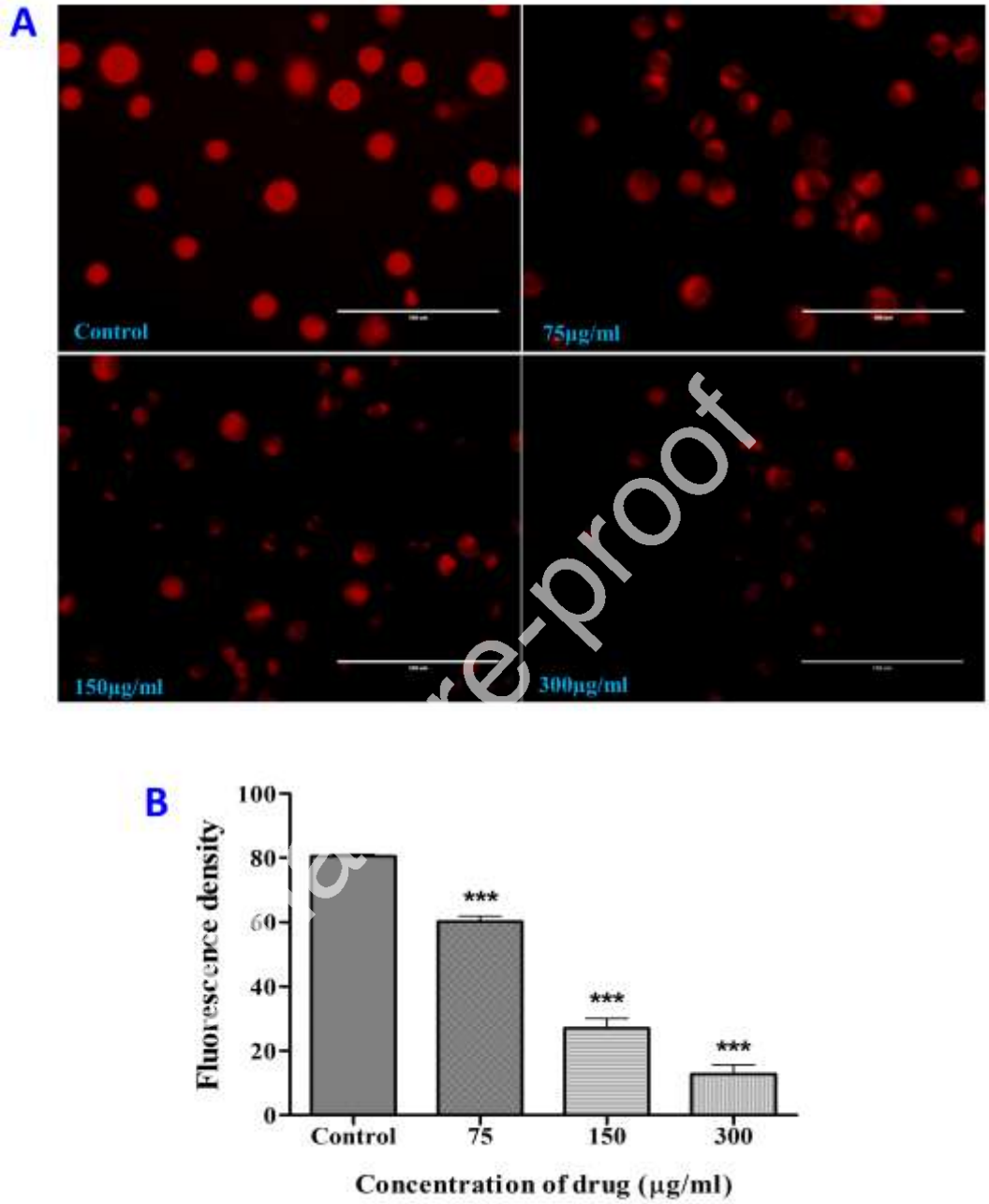


**Fig. 8**: (A) Rhodamine-123 staining exhibit that decreases in mitochondrial membrane potential after treating DL cells with Compound INH**9** for 24 hr and then analysed under fluorescence microscopy (×40 magnification). **(B)** Graph showing the density of Rhodamine-123 in a dose-dependent manner (significant at $^{***}p < 0.001$).

**3.8 Comparison of Antitumor activity of INH9**

There are very few publications on the antiproliferative properties of synthetic chemicals or metal complexes against DL cells. The antitumor activity of the compound INH**9** against DL cells has been compared in terms of $IC_{50}$ values previously reported compounds/metal complexes/traditional extracts under alike conditions (Table 6) [29, 40-43]. The higher anticancer activity at a low dose is shown by a lower IC50 value. While, cis-platin has better anticancer action than INH**9** but platinum-based compounds are very costly, non-selective, and have side effects [44]. Hppo is a more complex molecule that involves a number of starting materials and multistep synthesis, whereas INH**9** is synthesized more conveniently by a single step with only two starting materials. Ruthenium and iridium complexes are not cost-efficient and again involve multistep synthesis. The antitumor activity of INH8 is much better than medicinal extracts Garcinia morella and Dendrobium formosum. The better activity of INH**9** may be attributed to the isoniazid core and $NH_2$ interaction site [45].

**Table 6.** $IC_{50}$ value of INH**9** and previously reported compounds/metal complexes/extracts.

| **Compounds/Complexes/Extracts** | **$IC_{50}$ values (µg/mL) [26, 37-40]** |
|---|---|
| Cis-platin | 1 |
| 5(4-hydroxyphenyl)-2-(N-phenylamino)-1,3,4-oxadiazole | 50 |
| Doxorubicin | 70.52 (or 129.3 µM) |
| Rh-Complex | 20-30 |
| Ru-Complex-1 | >110 |
| Ru-Complex-2 | 100-110 |
| Ru-Complex-3 | 80-90 |
| Ir-Complex | >110 |
| Garcinia morella | 250 |
| Ethanolic Extract of Dendrobium formosum | 350 |

| | |
|---|---|
| **INH9** | 150 |

## 4. Conclusion

Here, compounds INH**1-9** have been synthesized and fully characterized. The UV-vis spectrum of INH**1-9** shows corresponding bands owing to π→π* transition, which is further confirmed by TD-DFT calculations. A small energy gap between the HOMO and LUMO of these compounds indicates their softness and high reactivity. The crystal structure of INH**4**, INH**8,** and INH**9** shows the presence of various intermolecular interactions that are further verified by Hirshfeld surface analysis. The molecular docking study suggested that compounds INH1-9 have the potential to bind with MDM2 protein, which can lead to inhibition of p53–MDM2 interaction thereby restoring of activity of tumor suppressor protein p53. Among the various derivatives, INH**9** binds most strongly with the target protein. *In-vitro* anticancer activities of lead compound INH**9** against Dalton's Lymphoma revealed that the synthesized compound INH**9** exhibits a potent anticancer and anti-proliferative activity in an optimum dose and time-dependent kinetics. In addition, these findings also elucidate cell shrinkage, chromatin condensation, nuclear fragmentation, and membrane blebbing which are hallmarks of apoptosis, as well as intracellular ROS generation and mitochondrial membrane potential. It induces apoptosis with increased ROS production and also reduces the mitochondrial membrane potential of Dalton's lymphoma cells *in vitro* conditions. Therefore, these current investigations will appreciably participate in designing anticancer therapeutic drugs based on INH derivatives. These synthesized Schiff bases also have preferable binding sites that can be utilized for the synthesis of metal complexes based on these.

**ACKNOWLEDGMENT**

Dr M K Bharty acknowledges BHU, Varanasi, for providing a research grant IoE Dev. Scheme No. 6031 for the study and characterization of the designed compound and its application. Shivendra Kumar Pandey thank UGC India for JRF award.

**Supplementary material**

Supplementary crystallographic data for Compounds INH**4**, INH**8**, and INH**9** can be obtained through CCDC 2234056, 2240162, and 2240730, respectively. Other supplementary materials for this article can be found, in the online version, at http://dx.doi.org/.

**References**

1. J. Ferlay, M. Ervik, F. Lam, M. Colombet, L. Mery, M. Piñeros, A. Znaor, I. Soerjomataram, F. Bray, Global Cancer Observatory: Cancer Today, Lyon: International Agency for Research on Cancer (2020).
2. S. K. Aggarwal, A histochemical approach to the mechanism of action of cisplatin and its analogues, J. Histochem. Cytochem. 41 (1993) 1053–1073.
3. A. Brozovic, A. Ambriovic-Ristov, M. Osmak, The relationship between cisplatin-induced reactive oxygen species, glutathione, and BCL-2 and resistance to cisplatin, Crit. Rev. Toxicol. 40 (2010) 347–359.
4. A. L. Demain, P. Vaishnav, Natural products for cancer chemotherapy, Microb. Biotechnol. 4 (2011) 687-99.
5. T. L. Blundell, Structure-Based Drug Design, Nature 384 (1996) 23-26.
6. S. Kalyaanamoorthy, Y.-P. P. Chen. Structure-Based Drug Design to Augment Hit Discovery, Drug Discovery Today 16 (2011) 831-839.
7. S. S. Swain, S. K. Paidesetty, R. N. Padhy, T. Hussain, Isoniazid-phytochemical conjugation: A new approach for potent and less toxic anti-TB drug development, Chem. Biol. Drug Des. 96 (2020) 714-730.

8. V. Judge, B. Narasimhan, M. Ahuja, D. Sriram, P. Yogeeswar, Isonicotinic acid hydrazide derivatives: synthesis, antimycobacterial, antiviral, antimicrobial activity and QSAR studies, Letters in Drug Design & Discovery 8 (2011) 792-810.
9. H. A. R. Mohamed, A. H. Mostafa, M. M. Heba, M. H. Nasser, Synthesis, characterization, molecular docking and cytotoxicity studies on N-benzyl-2-isonicotinoylhydrazine-1 carbothioamide and its metal complexes, J. Mol. Struct. 1196 (2019) 417-428.
10. A. Muhib, R. Denise, M. Malachy, D. Michael, T. Brendan, C. M. G. Anna, S. S. Leandro, O. P. S. Lucieri, C. L. Maria, G. Karen, S. D. S. Andre-Luis, Synthesis and antimicrobial activity of a phenanthrolineisoniazid hybrid ligand and its Ag+ and Mn2+ complexes, Biometals. 32 (2019) 671–682.
11. G. dos SS Firmino, S. C. Andre, Z. Hastenreiter, V. K. Campos, M. A. Abdel-Salam, E. M. de Souza-Fagundes, J. A. Lessa, In vitro assessment of the cytotoxicity of Gallium (III) complexes with Isoniazid-Derived Hydrazones: Effects on clonogenic survival of HCT-116 cells, Inorganica Chimica Acta 497 (2019) 119079.
12. C. R. F. Maria, M. S. A. Joseneide, L. Z. Roberta, I. Y. Maria, A. R. Nicolás, D. Renata, Synthesis and structural characterization of a zinc(II) complex of the mycobactericidal drug isoniazid –Toxicity against Artemiasalina, Polyhedron 30 (2011) 1922–1926.
13. H. Kargar, M. Fallah-Mehrjardi, R. Behjatmanesh-Ardakani, K. S. Munawar, M. Ashfaq, M. N. Tahir, Diverse coordination of isoniazid hydrazone Schiff base ligand towards iron (III): Synthesis, characterization, SC-XRD, HSA, QTAIM, MEP, NCI, NBO and DFT study, J. Mol. Struct. 1250 (2022) 131691.

14. V. Ferraresi-Curotto, G. A. Echeverría, O. E. Piro, R. Pis-Diez, A. C. González-Baró, Synthesis and characterization of a series of isoniazid hydrazones. Spectroscopic and theoretical study. J. Mol. Struct. 1133 (2017) 436-47.
15. A. C. González-Baró, R. Pis-Diez, B. S. Parajón-Costa, N. A. Rey, Spectroscopic and theoretical study of the o-vanillin hydrazone of the mycobactericidal drug isoniazid, J. Mol. Struct. 1007 (2012) 95-101.
16. D. Sriram, P. Yogeeswari, K. Madhu, Synthesis and in vitro and in vivo antimycobacterial activity of isonicotinoyl hydrazones. Bioorganic & medicinal chemistry letters 15(20) (2005) 4502-5.
17. M. Iqbal, M. A. Bhat, F. Shakeel, Development and validation of UHPLC- MS/MS assay for rapid determination of a carvone Schiff base of isoniazid (CSB- INH) in rat plasma: Application to pharmacokinetic study. Biomedical Chromatography 29(6) (2015) 876-82.
18. Y. Q. Hu, S. Zhang, F. Zhao, C. Gao, L. S. Feng, Z. S. Lv, Z. Xu, X. Wu, Isoniazid derivatives and their anti-tubercular activity. Eur. J. Med. Chem. 133 (2017) 255-67.
19. V. Judge, B. Narasimhan, M. Ahuja, Isoniazid: the magic molecule. Med. Chem. Research 21 (2012) 3940-57.
20. H. Kumar, D. Malhotra, R. Sharma, E. Sausville, M. Malhotra, Synthesis, Characterization and Evaluation of Isoniazid Analogues as Potent Anticancer Agents, Pharmacologyonline 3 (2011) 337-343.
21. B. A. Al-Hiyari, A. K. Shakya, R. R. Naik, S. Bardaweel, Microwave-assisted synthesis of Schiff bases of isoniazid and evaluation of their anti-proliferative and antibacterial activities. Molbank 1 (2021) M1189.

22. M. J. Turner, J. J. McKinnon, S. K. Wolff, D. J. Grimwood, P. R. Spackman, D. Jayatilaka, M. A. Spackman. CrystalExplorer (Version 17.5) University of Western Australia: Crawley Australia, (2017).

23. M. J. Frisch, G. W. Trucks, H. B. Schlegel, G. E. Scuseria, M. A. Robb, J. R. Cheeseman, G. Scalmani, V. Barone, B. Mennucci, G. Petersson, H. Nakatsuji, gaussian 09, Revision d. 01, Gaussian. Inc., Wallingford CT 2009.

24. L. J. Bartolottiand, K. Fluchick, in *Reviews in computational chemistry*, ed. K. B. Lipkowitz, D. Boyd, VCH, New York 7 (1996) 187-216.

25. C. Lee, W. Yang, R. G. Parr, Development of the colle-salvetti correlation-energy formula into a functional of the electron density, Phys. Rev. B: Condens. Matter. 37 (1988) 785-789.

26. G. M. Morris, R. Huey, W. Lindstrom, M. F. Sanner, R. K. Belew, D. S. Goodsell, A. J. Olson, Autodock 4 and AutoDockTools4: automated docking with selective receptor flexiblity, *J. Computational Chem.* **16** (2009) 2785-91.

27. R. Chaurasia, S. K. Pandey, D. K. Singh, M. K. Bharty, V. Ganesan, S. K. Hira, P. P. Manna, A. Bharty, R. J. Butcher, Antiproliferative activity and electrochemical oxygen evolution by Ni (II) complexes of N'-(aroyl)-hydrazine carbodithioates. Dalton Trans. (2021). https://doi.org/10.1039/D1DT02285G

28. D. Tang, D. Wu, A. Hirao, J. M. Lahti, L. Liu, B. Mazza, V. J. Kidd, T. W. Mak, A. J. Ingram, ERK activation mediates cell cycle arrest and apoptosis after DNA damage independently of p53, J. Biol. Chem. 277 (2002) 12710–7.

29. M. K. Gond, A. Shukla, S. K. Pandey, M. K. Bharty, B. Maiti, A. Acharya, N. Tiwari, D. Katiyar, R. J. Butcher, Mn(II) catalyzed synthesis of 5(4-hydroxyphenyl)-2-(N-phenylamino)-1,3,4-oxadiazole: Crystal structure, DFT, Molecular docking, Hirshfeld

surface analysis, and in vitro anticancer activity on DL cells, J. Mol. Struc. 1249 (2022) 131547.

30. P. Gautam, O. Prakash, R. K. Dani, M. K. Bharty, N. K. Singh, R. K. Singh, Spectra-structure correlation-based study of complex molecules of 1-isonicotinoyl-3-thiosemicarbazide with Ni2+, Mn2+ and Fe3+ using Raman, UV–visible and DFT techniques, J. Mol. Struct. 1127 (2017) 489-497.

31. Q L Deng, M Yu, X hen, H Diao, Z L Jing, Z Fan, N′-(4-Hydroxybenzylidene) isonicotinohydrazide, Acta Crystallographica Section E: Structure Reports Online. 61(8) (2005) o2545-6.

32. S. Jaiswal, S. K. Pandey, T. Minocha, S. Chandra, M. K. Bharty, S. K. Yadav, D. Kushwaha, R. J. Butcher, Mn (II) assisted synthesis of N-phenyl-5-(pyridin-3-yl)-1, 3, 4-oxadiazol-2-amine and evaluation of its antiproliferative activity, J. Mol. Struct. 1281 (2023) 135075.

33. M. K. Gond, S. K. Pandey, S. Chandra, N. Tiwari, M. K. Bharty, B. Maiti, D. Katiyar, R. J. Butcher, Zinc (II) catalyzed synthesis of 2-(4-methoxyphenyl)-5-(2-pyridyl)-1, 3, 4-thiadiazole: Characterizations, crystal structure, DFT calculation, Hirshfeld surface analysis, and molecular docking analysis. J. Mol. Struct. 1267 (2022) 133586.

34. S. Selvaraj, P. Rajkumar, M. Kesavan, K. Thirunavukkarasu, S. Gunasekaran, N. Saradha Devi, S. Kumaresan, Spectroscopic and structural investigations on modafinil by FT-IR, FT-Raman, NMR, UV–Vis and DFT methods, Spectrochim. Acta Part A 224 (2020) 117449.

35. T. K. Roy, Jr T. Carrington, R. B. Gerber, Approximate first-principles anharmonic calculations of polyatomic spectra using MP2 and B3LYP potentials: comparisons with experiment, J. Phy. Chem. A 118 (2014) 6730-6739.

36. K. Fukui, Role of frontier orbitals in chemical reactions, Science 218 (1982) 747-754.

37. D. F. Perepichka, M. R. Bryce, Molecules with exceptionally small HOMO–LUMO gaps, Angew. Chem. Int. Ed. 44 (2005) 5370-5373.

38. A. Lauria, M. Tutone, M. Ippolito, L. Pantano, A. M. Almerico, Molecular modelling approaches in the discovery of new drugs for anti-cancer therapy: the investigation of p53–MDM2 interaction and its inhibition by small molecules, Curr. Med. Chem. 17 (2010) 3142–3154.

39. W. Wang, Y. Hu, Small molecule agents targeting the p53–MDM2 pathway for cancer therapy, Med. Res. Rev. 32 (2011) 1159-1196.

40. R. P. Paitandi, R. K. Gupta, R. S. Singh, G. Sharma, B. Koch, D. S. Pandey, Interaction of ferrocene appended Ru(II), Rh(III) and Ir(III) dipyrrinato complexes with DNA/protein, molecular docking and antitumor activity, Eur. J. Med. Chem. 84 (2014) 17-29.

41. P. Srivastava, S. K. Hira, D. N. Srivastava, V. K. Singh, U. Gupta, R. Singh, R. A. Singh, P. P. Manna, ATP-Decorated mesoporous silica for biomineralization of calcium carbonate and p2 purinergic receptor-mediated antitumor activity against aggressive lymphoma, ACS Appl. Mat. Interfaces 10 (2018) 6917–6929.

42. R. Prasad, B. Koch, Antitumor activity of ethanolic extract of Dendrobium formosum in T-cell lymphoma: an in vitro and in vivo study, BioMed research international (2014).

43. B. Choudhury, R. Kandimalla, R. Bharali, J. Monisha, A. B. Kunnumakara, K. Kalita, J. Kotoky, Anticancer activity of Garcinia morella on T-cell murine lymphoma via apoptotic induction, Front. Pharmacol. 7 (2016) 3.

44. D. Wang, S. Lippard, Cellular processing of platinum anticancer drugs, Nat. Rev. Drug. Discov. 4 (2005) 307–320.

45. A. K. Jain, C. Karthikeyan, K. D. McIntosh, A. K. Tiwari, P. Trivedi, A. DuttKonar, Unravelling the potency of 4,5-diamino-4H-1,2,4 triazole-3-thiol derivatives for kinase inhibition using a rational approach, New J. Chem. 43 (2019) 1202-1215.

## Credit author

**Seema Gupta: Methodology,** Data curation, Formal Analysis, Writing- Original draft preparation

**Shivendra Kumar Pandey:** Methodology, Data curation, Investigation, Software, Visualization, Formal analysis, Writing- Original draft preparation

**Sandeep Kumar:** Methodology, Data curation, Investigation, Software, Visualization, Writing- Original draft preparation

**Ram Nayan Gautam**: Formal Analysis, Writing- Reviewing and Editing

**A. K. Patel**: Writing- Reviewing and Editing

**M. K. Bharty: Conceptualization,** Supervision**,** Resources, Project administration, Funding acquisition, Formal analysis, Validation**,** Writing- Reviewing and Editing

**D. Kushwaha:** Methodology, Data curation, investigation, Writing- Reviewing and Editing

**A. Acharya:** Supervision**,** Writing- Reviewing and Editing

**R. J. Butcher**: Methodology, Data curation

## Graphical abstract

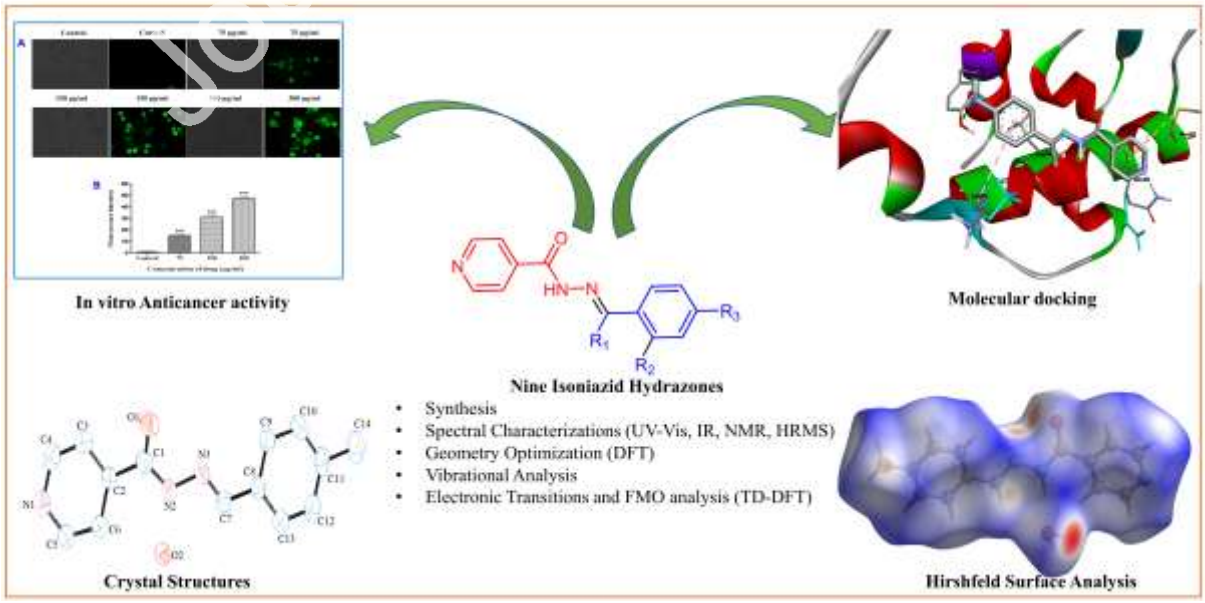

**Declaration of Competing Interest**

◉ The authors declare that they have no known competing financial interests or personal relationships that could have appeared to influence the work reported in this paper.

☐The authors declare the following financial interests/personal relationships which may be considered as potential competing interests: